nature geoscience

LETTERS

PUBLISHED ONLINE: 17 MARCH 2013 | DOI: 10.1038/NGEO1759

Flash vaporization during earthquakes evidenced by gold deposits

Dion K. Weatherley[1]* and Richard W. Henley[2]

Much of the world's known gold has been derived from arrays of quartz veins. The veins formed during periods of mountain building that occurred as long as 3 billion years ago[1–3], and were deposited by very large volumes of water that flowed along deep, seismically active faults. The veins formed under fluctuating pressures[4,5] during earthquakes[6], but the magnitude of the pressure fluctuations and their influence on mineral deposition is not known. Here we use a simple thermo-mechanical piston model to calculate the drop in fluid pressure experienced by a fluid-filled fault cavity during an earthquake. The geometry of the model is constrained using measurements of typical fault jogs, such as those preserved in the Revenge gold deposit in Western Australia[7], and other gold deposits around the world. We find that cavity expansion generates extreme reductions in pressure that cause the fluid that is trapped in the jog to expand to a very low-density vapour. Such flash vaporization of the fluid results in the rapid co-deposition of silica with a range of trace elements to form gold-enriched quartz veins. Flash vaporization continues as more fluid flows towards the newly expanded cavity, until the pressure in the cavity eventually recovers to ambient conditions. Multiple earthquakes progressively build economic-grade gold deposits.

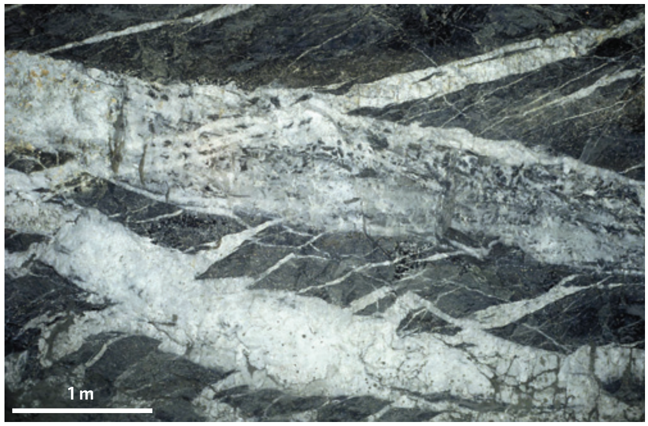

Figure 1 | Gold–quartz extensional veins. Typical complex of veins that records episodes of fluid flow due to successive fault failures (Defiance lode system[6], St Ives, Eastern Goldfields, Western Australia). Photograph printed with permission from S. F. Cox (Australian National University).

A long-standing question about the world's gold resources—the resource that by chance of history underpins much of our global economy—is how the metal becomes concentrated from a crustal abundance of about 2 parts per 10^9 (ppb) to form highly localized, mineable deposits with gold concentrations more than a thousand times higher. About one third of these resources[8] occur as mesothermal gold–quartz veins (Fig. 1) whose formation, in general terms, is well established to be a consequence of the release of water from sedimentary–volcanic rock sequences as they pass through the orogenic cycle of burial, metamorphism and subsequent uplift and erosion[9], sometimes with evidence of associated magmatism. These veins, along with often extensive silicification and carbonate–pyrite host rock alteration, are clearly tied to cycles of fracture permeability through a repetitive sequence of brittle or brittle-shear failure along major fault systems and choking of new fractures by mineral deposition[10]. This local cycling of rupture and increased fluid flow to form gold–quartz veins is readily linked to changes in fluid pressure through the earthquake rupture and aftershock cycle[6], but what is not so clear is the magnitude of those changes or how they may drive the process of gold mineralization. As fluid flux at any scale is a function of permeability and pressure gradient, we therefore start with a simple question. Figure 2a shows a quartz-filled jog that is typical in fault-related gold mineralization[7]; ambient conditions before failure were estimated, from mineral phase relations, as ∼390 °C at a depth of ∼11 km, corresponding to a lithostatic pressure of ∼290 MPa (ref. 11), but what was the fluid pressure in the fracture immediately post rupture?

Figure 2b provides a simple piston model of a vertical strike-slip fault containing a jog whose long axis is oriented perpendicular to the slip-direction of the fault (for detail see Methods). If rupture on the fault is initiated remotely from the jog and driven primarily by accumulation of tectonic stress until the frictional strength of the fault is exceeded, we may estimate the change in volume within the jog due to the action of an earthquake of a prescribed seismic moment[12]. Assuming that water fully occupied the initial jog volume (with an initial aperture width, $d \sim 100\,\mu$m), its pressure, P_f, would change, consequent on a magnitude 4 displacement (slip = 0.13 m), from an ambient 290 MPa to only 0.2 MPa immediately following failure (Fig. 3a). In contrast, the minimum fluid pressure (P_{fm}) post-failure is commonly assumed to be constrained close to hydrostatic pressure (110 MPa in this example). While this assumption is reasonable for open fracture arrays that maintain a fluid-filled continuum in the upper few kilometres of the seismogenic crust, it is not appropriate for metamorphic rocks at greater depth during orogeny. Figure 3b compares the minimum fluid pressures for a range of earthquake magnitudes relative to initial fluid lithostatic pressure. These data show that major fluid pressure drops occur for even very small

[1]WH Bryan Mining and Geology Research Centre, Sustainable Minerals Institute, The University of Queensland, Brisbane, Queensland 4072, Australia, [2]Research School of Earth Sciences, Australian National University, Canberra, Australian Capital Territory 0200, Australia.
*e-mail: d.weatherley@uq.edu.au.

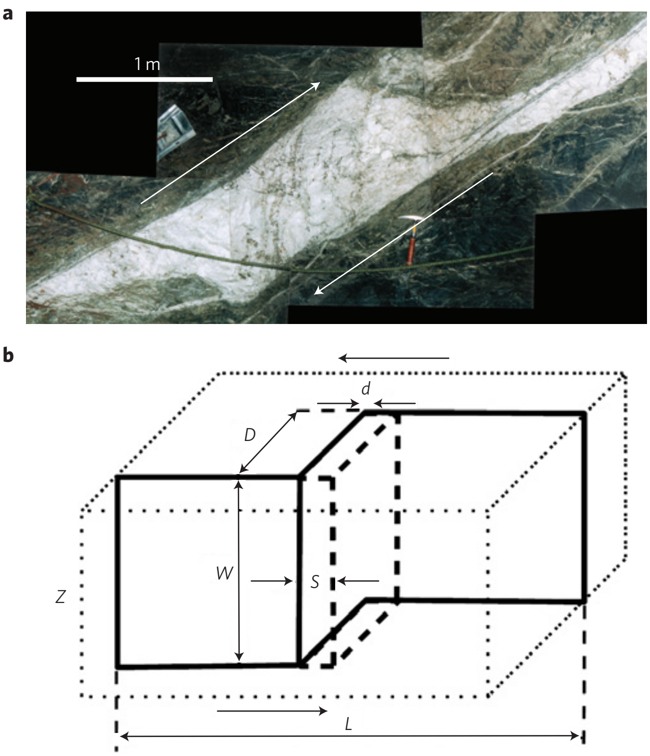

Figure 2 | Opening of jogs on faults during earthquakes[7] showing relative motion of the sidewalls during slip. a, Example of a quartz-filled dilational jog in a shear vein at the Archaean Revenge gold deposit (Kambalda, Western Australia). **b**, A simple block model for analysis of rate of change of volume and fluid pressure due to seismic slip. Annotations refer to block and slip dimensions as described in the Methods. Photograph printed with permission from S. F. Cox (Australian National University).

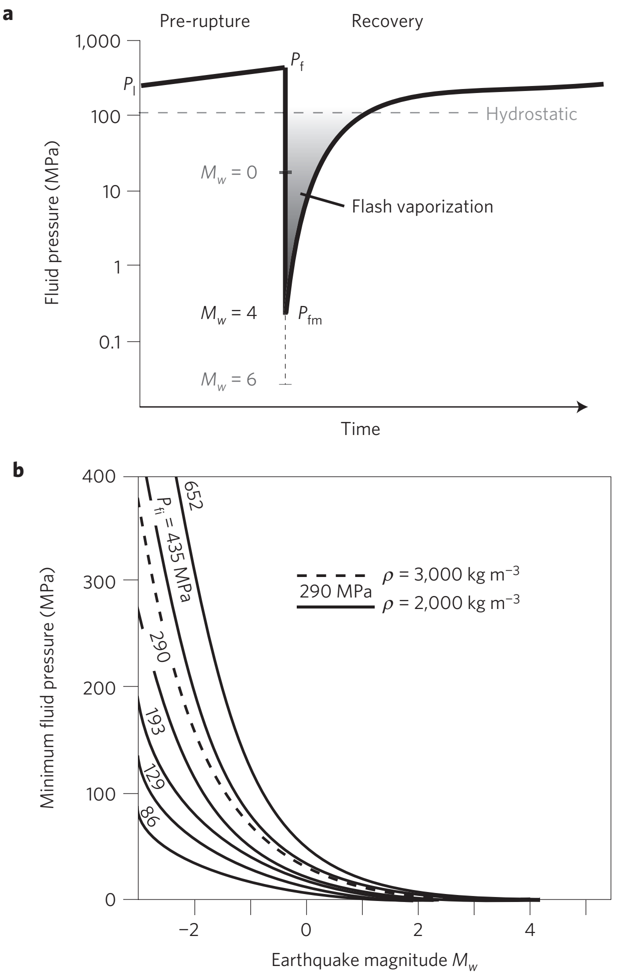

Figure 3 | Fluid pressure transients during earthquakes. a, Fluid pressure transient during a magnitude 4 earthquake cycle. In the pre-rupture stage, deviatoric crustal stress increases pore fluid pressure (P_f) in the incipient rupture relative to lithostatic pressure (P_l) until failure occurs. Fluid expansion occurs with the initiation of flash vaporization, immediately achieving minimum fluid pressure (P_{fm}) in the slip volume of the jog. During the recovery stage fluid from the surrounding rock flows into and through the very low-pressure jog regime until fluid pressure is restored to the ambient lithostatic condition when $P_f = P_l$. Flash vaporization of the input fluid occurs in the jog and feeder fracture arrays throughout most of this recovery period. The hydrostatic pressure equivalent to the initial pressure is shown only for reference. **b**, Minimum fluid pressure immediately following dilation of fault jogs as a function of earthquake magnitude. These curves are drawn for the lower bound of rock densities in the crust ($\rho = 2{,}000\ \mathrm{kg\ m^{-3}}$) and the upper bound ($\rho = 3{,}000\ \mathrm{kg\ m^{-3}}$) is illustrated for the initial condition of 290 MPa.

displacement slips at low magnitudes. The piston model therefore provides a more appropriate basis for initialization of detailed models of post-seismic fluid pressure recovery than assumptions of zero fluid pressure[13] and incompressible flow.

Evidence for pressure fluctuations during vein formation has been provided through detailed fluid inclusion data on vein quartz[4,5]. Our first-order analysis shows that the volume change due to dilation on a jog ranges, relative to the initial aperture volume of the fracture, from about 130 times for a magnitude 2 earthquake, to 13,000 for a magnitude 6. Figure 4a shows the extent of fluid decompression for this example. Relative to the ambient conditions pre-failure, the fluid phase expands by several orders of magnitude to a very low-density compressible fluid, an irreversible, single-phase process that in chemical engineering terms is termed flash vaporization. The process at the scale of the jog and its surroundings is isothermal owing to the thermal mass of the rock and the high surface area of wallrock exposed to fluid.

Flash vaporization due to slip has not been previously recognized as a major driver of mineralization. It applies to any extensional vein setting whether in strike-slip, normal or thrust faults regardless of the source of fluid. Moreover, its effect is not limited to the small finite volume of the jog itself because, in combination with fault damage and other fractures, at the local and regional scales, the instantaneous insertion of ultralow-pressure sinks along an arterial fault inevitably translates as a decompression wave and consequent fluid flow response through a much larger fracture network that is highly sensitive to stress perturbations[6,14,15]. The extreme fluid pressure oscillations due to each slip event are also the likely root cause of processes such as fluid mixing[16] and redox change that contribute variously to mineral deposition in fault-hosted mineral deposits.

Flash vaporization is a consequence of extreme pressure transients due to slip events in fault arrays. Such extreme changes in fluid pressure translate immediately through equivalent extreme change in fluid density, into a cascade of coupled, nonlinear chemical responses in the decompressed fluid, and it is these that result in the mineral assemblages and textures that characterize veins. Recent experimental data have shown that precious metal solubilities are strongly dependent on fluid pressure[17] ensuring fast and efficient co-precipitation of gold and silver with silica during each seismic event as a consequence of the flash-induced supersaturation. Auriferous quartz–carbonate veins commonly also contain rutile, scheelite ($CaWO_4$), pyrite (FeS_2) and arsenopyrite (FeAsS), with bismuth and tellurium, so that, as well as being

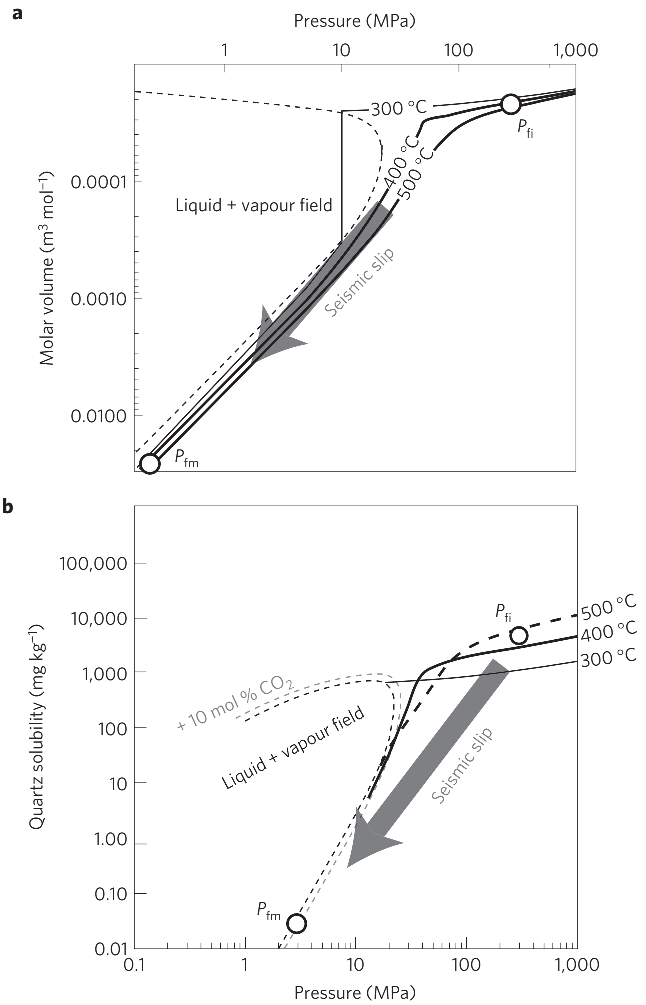

Figure 4 | Fluid density and quartz solubility transients during earthquakes. a, Pressure–molar volume relations for pure water. These data approximate fluids typical of mesothermal vein environments ($\ll$ 8 wt% NaCl solution with less than 10 mol% CO_2). **b**, Solubility of quartz (SiO_2) in pure water as a function of pressure and temperature. P_{fi} and P_{fm} are the fluid pressures relating to the jog shown in Fig. 2a and illustrate the extreme supersaturation ($\sim 10^5$) due to flash vaporization during rupture. At high supersaturations, silica nucleates to nanoparticles (<100 nm) that subsequently mature through a range of possible metastable silica hydrate phases. In **a**,**b** the general decompression vector is shown by the broad arrows.

a tracer of major water flows through the crust, gold deposits record the dispersion of the minor and trace elements (Au, Ag, As, Sb, B, Se, Te, Bi, W and Mo) that are incompatible with the evolving mineral assemblages in the metamorphic source rocks[18]. As the solubilities of most common rock-forming and ore minerals in aqueous solutions under mid-crustal conditions are primarily dependent on the density of water[19], this suite of vein components is linked directly to P_{fm} during the brittle failure cycle through the destabilization of solvated molecular species including $As(OH)_3$, $B(OH)_3$, H_2MoO_4 and H_2WO_4.

Flash vaporization is a highly efficient mechanism for the characteristic co-precipitation of silica with metals during vein formation. Quartz solubility, predominantly due to the solvated molecular species, $Si(OH)_{4,aq}$, is strongly density, and therefore pressure, dependent (Fig. 4b) primarily owing to changes in the degree of polymerization of water molecules. At 300 MPa and 450 °C, for example, its solubility is about 4,200 mg kg^{-1} but drops below 0.03 mg kg^{-1} on flash decompression to less than 1 MPa (ref. 19). It is this extreme supersaturation (>140,000 in this example) relative to quartz that drives silica deposition, through a succession of metastable polymorphs including hydrated silica phases[20], during each decompression cycle of vein formation. Very rapid flash precipitation of silica is known to occur first to nanoscale particles[21], followed by particle clustering[22,23] and eventual conversion to crystalline quartz. This *post facto* sequence severely limits the utility of fluid inclusion data in determining post-failure pressure–temperature-composition conditions. The mineral assemblages and textures that are preserved in and around veins, along with fluid inclusions and distinctive stable isotope distributions, are then the record of fluid pressure recovery and retrograde changes[24] rather than primary deposition conditions. Entrapment of CO_2-rich fluids in inclusions in some vein systems, for example, may be a consequence of localized phase separation from an initial low-CO_2 phase during pressure recovery and silica recrystallization, rather than evidence of the availability of a much larger reservoir of CO_2-rich fluid.

Isolated slips do not, of course, generate economically viable gold deposits. Assuming that the gold content of a quartz-saturated fluid trapped in the initial jog was 0.1–1 mg kg^{-1} (ref. 10), the mass of gold deposited in each event (10^{-2}–10^{-1} mg m^{-2} of the slip surface) is directly related to the slip volume and, as a function of earthquake magnitude, the strike length of the rupture zone on the parent fault. Flash vaporization immediately consequent on slip would therefore yield only a thin coating of silica–gold vein material with a high concentration of gold ($\sim$0.025–0.25 g kg^{-1})—albeit, economically, a very high grade ($\sim$1–10 ounces per tonne). It is the subsequent recovery stage flow of fluid from the surroundings into and through the jog that progressively builds the mass of vein material cycle by cycle. It is therefore the repetitiveness of the slip–recovery cycle in a regional-scale fault system that, initiated by flash vaporization, integrates through to the generation of economically viable gold deposits. This relationship enables a crude approximation to be made for the time taken to form a major (100 tonne Au) mesothermal gold vein deposit during an orogenic cycle. Assuming a seismic frequency history similar to that of, for example, the Alpine Fault system in the Southern Alps, New Zealand[25], the formation of one such deposit would take much less than 100,000 years.

Multiple repetitive slip events localized by fault geometry in combination with highly efficient flash vaporization are the key to understanding how gold becomes concentrated from extremely low crustal abundance to form economic deposits. The huge, late Paleozoic, Muruntau (Uzbekistan) deposit, for example, is a consequence of multiple rupture events that deposited over 6,000 tonnes of gold; 80% occurs in small-scale dislocations and 20% in large extension veins[26]. At an average abundance of 2 ppb, this mass of gold is equivalent to the gold content of more than 1,000 km^3 of average crustal rock, yet has become concentrated into a highly silicified volume of rock of less than 10 km^3. If only a few per cent of the crustal gold is extracted, or in the absence of efficient chemical deposition, the source volumes would have been orders of magnitude larger.

The recognition of the possibility of extreme pressure transients and flash vaporization in active fault arrays extends beyond the realm of economically viable vein deposits formed in ancient mountain belts. These account for 31% of global gold resources past and present with a further 45% residing in the Witwatersrand Basin (South Africa) that was derived arguably from veins in earlier mountain ranges[27]. Another 10% occurs in vein arrays such as the huge Grasberg (Indonesia) porphyry copper–gold deposit (>2,700 million tonnes of gold and 30 million tonnes of copper) that are variously associated with major magma-related fluid flux through the stressed seismogenic crust beneath ancient volcanoes. Flash vaporization consequent on seismic slip may therefore underpin the formation of more than 80% of the world's gold deposits; a simple repetitive process related to the everyday occurrence of earthquakes.

Methods

Using well-established relationships we provide a simple model for the change in volume within a fault jog due to the action of an earthquake of a prescribed seismic moment. Then assuming that the jog before rupture was occupied by fluid, the volume change is translated into a change in fluid pressure consequent on earthquake rupture.

Figure 2b is a simplified block model of a vertical strike-slip fault containing a step-over jog with symbols defining block and slip dimensions. The jog is oriented perpendicular to the slip direction of the fault and the sense of slip along the fault is such that an earthquake rupture will induce opening of the jog. Here it is assumed that rupture of the fault is initiated remotely from the jog and is primarily driven by tectonic stress accumulation until the frictional strength of the fault is exceeded. We aim to estimate the change in volume within the jog due to the action of an earthquake of a prescribed seismic moment[12],

$$M_o = \mu A s$$

where μ is the shear rigidity of the host rock (here assumed to be 30 GPa, a typical value for crustal rocks), A is the surface area of the rupture and s is the slip (or displacement) across the fault surface, averaged over the rupture area. As seismic moment (in units of Newton meters, N m) may be unfamiliar for some readers, herein seismic moments are converted to an equivalent moment magnitude[28],

$$M_w = 2/3 \log M_o - 10.7$$

The source dimensions of the earthquake are computed as a function of M_w using empirical scaling relations[29] for small-magnitude ($M_w < 4$) strike-slip earthquakes whose hypocentral depths range between 3.5 and 45 km. The rupture length (L) is given by:

$$\log M_o = 2.5 \log L + 7.85$$

or, in terms of moment magnitude:

$$2.5 \log L + 7.85 = 1.5(M_w + 10.7)$$

Having computed the rupture length, the down-dip width (W) of the rupture is computed according to established empirical relations: $W = L$ for small magnitude earthquakes ($M_w < 4.0$); $W = 15.0L^{2/3}$ for moderate earthquakes ($4.0 < M_w < 6.0$); $W = 17$ km, the mean crustal seismogenic width for large earthquakes ($M_w > 6.0$).

The average slip (s) is also computed as a function of rupture length:

$$\log s = 0.833 \log L - 3.84$$

Supplementary Table S1 provides estimates for rupture length, rupture width and average slip for various moment magnitudes. It also includes the relative volume change:

$$V_f/V_i = (V_i + \Delta V)/V_i = 1 + s/d$$

$$\Delta V = WDs$$

where W is the vertical extents of the jog, taken as equal to the down-dip width of the rupture; D is the step-over distance (or jog length) and assumed to be $D \sim 1$ m for subsequent calculations; d is an initial effective aperture thickness ($d \sim 100\,\mu$m).

It is convenient to assume for the first-order analysis of this model that the fluid phase behaves as an ideal gas with equation of state $PV = nRT$, so that for isothermal expansion at a temperature, T_i,

$$P_f V_f = P_i V_i$$

where P_i and V_i are the initial pressure and molar volume of water pre-rupture. The relative pressure change is then

$$P_f/P_i = V_i/V_f = 1/(1 + s/d)$$

The final pressure of the fluid isothermally expanded in a jog is tabulated in Supplementary Table S2 for various moment magnitudes and burial depths (z) of the fault. These tabulated pressures are a more appropriate initial condition for models of post-seismic fluid recovery than those assuming zero fluid pressure immediately following a seismic event[13]. The initial pressure of the fluid and its temperature before the earthquake are, neglecting the small component of tensile strength, computed as:

$$P_i(z) = \rho g z$$

where $\rho \sim 2\,000$ kg m^3 is a lower bound for crustal rocks, and $g \sim 9.81$ m s^{-2}.

$$T(z) = (\mathrm{d}T/\mathrm{d}z)z$$

and the thermal gradient ($\mathrm{d}T/\mathrm{d}z$) is taken as $\sim$40 °C km^{-1}.

Expansion in this model is assumed to be isothermal at the scale of the jog and its surroundings. This assumption is supported by production data for high-enthalpy geothermal wells[30] at depths of less than 4,000 m where phase separation occurs from initially vapour-saturated liquid water during discharge. In this much lower-pressure environment, isenthalpic expansion occurs across the two-phase boundary and is sustained by heat transfer from wallrock to fluid consequent on the decrease in temperature due to phase change. In the deeper, higher-pressure deep vein environments considered here instantaneous, irreversible isenthalpic expansion of the trapped fluid may occur at the micro-scale but with immediate restoration of temperature due to conduction through the high surface area of rock exposed to fluid[30].

Received 10 October 2012; accepted 7 February 2013; published online 17 March 2013

References

1. Sibson, R. H., Robert, F. & Poulsen, K. H. High-angle reverse faults, fluid-pressure cycling, and mesothermal gold–quartz deposits. *Geology* **16,** 551–555 (1988).
2. Boullier, A. M. & Robert, F. Paleoseismic events recorded in Archaean gold–quartz vein networks, Val d'Or, Abitibi, Quebec, Canada. *J. Struct. Geol.* **14,** 161–179 (1992).
3. Goldfarb, R., Baker, T., Dube, B., Groves, D. I., Hart, C. J. & Gosselin, P. Distribution, character and genesis of gold deposits in metamorphic terranes. *Econ. Geol.* **100th Anniversary Volume,** 407–450 (2005).
4. Wilkinson, J. J. & Johnston, J. D. Pressure fluctuations, phase separation, and gold precipitation during seismic fracture propagation. *Geology* **24,** 395–398 (1996).
5. Parry, W. T. Fault-fluid compositions from fluid-inclusion observations and solubilities of fracture-sealing minerals. *Tectonophysics* **290,** 1–26 (1998).
6. Cox, S. F. & Ruming, K. The St Ives mesothermal gold system, Western Australia—A case of golden aftershocks? *J. Struct. Geol.* **26,** 1109–1125 (2004).
7. Nguyen, P. T., Cox, S. F., Harris, L. B. & Powell, C. McA. Fault-valve behaviour in optimally oriented shear zones: An example at the Revenge gold mine, Kambalda, Western Australia. *J. Struct. Geol.* **20,** 1625–1640 (1998).
8. Frimmel, H. E. Earth's continental crust gold endowment. *Earth Planet. Sci. Lett.* **267,** 45–55 (2008).
9. Phillips, G. N. & Powell, R. Formation of gold deposits: A metamorphic devolatilization model. *J. Metamorph. Petrol.* **28,** 689–718 (2010).
10. Cox, S. F., Knackstedt, M. A. & Braun, J. in *Structural Controls on Ore Genesis* Vol. 14 (eds Richards, J. P. & Tosdal, R. M.) 1–24 (Society of Economic Geologists Review, Society of Economic Geologists, 2001).
11. Clark, M. E., Carmichael, M. D., Hodgson, C. J. & Fu, M. in *The Geology of Gold Deposits: The Perspective in 1988* (eds Keays, R. R., Ramsay, W. R. H. & Groves, D. I.) 445–459 (Economic Geology Monograph, Vol. 6, Society of Economic Geologists, 1989).
12. Aki, K. Generation and propagation of G waves from the Niigata earthquake of June 14, 1964. Part 2. Estimation of earthquake moment, released energy and stress-strain drop from G wave spectrum. *Bull. Earthq. Res. Inst.* **44,** 73–88 (1966).
13. Sheldon, H. A. & Ord, A. Evolution of porosity, permeability and fluid pressure in dilatant faults post-failure: Implications for fluid flow and mineralization. *Geofluids* **5,** 272–288 (2005).
14. Cox, S. F. Coupling between deformation, fluid pressures and fluid flow in ore-producing hydrothermal environments. *Econ. Geol.* **100th Anniversary Volume,** 39–75 (2005).
15. Shelly, D. R. Migrating tremors illuminate complex deformation beneath the seismogenic San Andreas fault. *Nature* **463,** 648–653 (2010).
16. Boiron, M. C., Cathelineau, M., Banks, D. A., Fourcade, S. & Vallance, J. Mixing of metamorphic and surficial fluids during the uplift of the Hercynian upper crust: Consequences for gold deposition. *Chem. Geol.* **194,** 119–141 (2003).
17. Migdisov, A. A. & Williams-Jones, A. E. A predictive model for metal transport of silver chloride by aqueous vapour in ore-forming magmatic-hydrothermal systems. *Geochim. Cosmochim. Acta* **104,** 123–135 (2013).
18. Pitcairn, I. K., Teagle, D. A. H., Craw, D., Olivo, G. R., Kerrich, R. & Brewer, T. S. Sources of metals and fluids in orogenic gold deposits: insights from the Otago and Alpine Schists, New Zealand. *Econ. Geol.* **101,** 1525–1546 (2006).
19. Dolejs, D. & Manning, C. E. Thermodynamic model for mineral solubility in aqueous fluids: Theory, calibration and application to model fluid-flow systems. *Geofluids* **10,** 20–40 (2010).
20. Tanner, D., Henley, R. W., Mavrogenes, J. A. & Mernagh, T. in XVI Congreso Peruano de Geologia SEG 2012 Conf. Lima, September 23–26, Poster 100 (Society of Economic Geologists, 2012).

21. Kind, M. & Kaiser, R. Flash Crystallization—A new process for designing crystalline powders. *17th Int. Symp. Industrial Crystallization* Vol. 1, 111–118 (Society of Economic Geologists, 2008).
22. Kind, M. Colloidal aspects of precipitation processes. *Chem. Eng. Sci.* **57,** 4287–4293 (2002).
23. Herrington, R. J. & Wilkinson, J. J. Colloidal gold and silica in mesothermal vein systems. *Geology* **21,** 539–542 (1993).
24. Vityk, M. O. & Bodnar, R. J. Textural evolution of synthetic fluid inclusions in quartz during reequilibration, with applications to tectonic reconstruction. *Contrib. Mineral. Petrol.* **121,** 309–323 (1995).
25. Robinson, R. Potential earthquake triggering in a complex fault network: The northern South Island, New Zealand. *Geophys. J. Int.* **159,** 734–748 (2004).
26. Drew, L. J., Berger, B. R. & Kurbanov, N. K. Geology and structural evolution of the Muruntau gold deposit, Kyzylkum Desert, Uzbekistan. *Ore Geol. Rev.* **11,** 175–196 (1996).
27. Frimmel, H. E. & Minter, W. E. L. Recent developments concerning the geological history and genesis of the witwatersrand gold deposits, South Africa. *Soc. Econ. Geol. Special Publ.* **9,** 17–45 (2002).
28. Hanks, T. C. & Kanamori, H. A moment magnitude scale. *J. Geophys. Res.* **84,** B2348–B2350 (1979).
29. Leonard, L. Earthquake fault scaling: Self-consistent relating of rupture length, width, average displacement, and moment release. *Bull. Seismol. Soc. Am.* **100,** 1971–1988 (2010).
30. Henley, R. W. & Hughes, G. O. Underground fumaroles: 'Excess heat' effects in vein formation. *Econ. Geol.* **95,** 453–466 (2000).

Acknowledgements
R.W.H. wishes to express his thanks to S. Cox and B. Berger for their constructive comments on this paper and stimulating discussions over several decades. D.K.W. would like to thank R.W.H., D. Wood and his colleagues at the W. H. Bryan Mining and Geology Research Centre for encouragement to consider seismological implications for mineral deposition. D. Tanner also kindly provided constructive comments.

Author contributions
R.W.H. conceived the initial concept. D.K.W. carried out the analysis and both authors contributed to the writing.

Additional information
Supplementary information is available in the online version of the paper. Reprints and permissions information is available online at www.nature.com/reprints. Correspondence and requests for materials should be addressed to D.K.W.

Competing financial interests
The authors declare no competing financial interests.